Multifunctional magnetic rotator for micro and nanorheological studies

Alexander Tokarev,[1] Alexey Aprelev,[2] Mikhail N. Zakharov,[2,3] Guzeliya Korneva,[4,5] Yury Gogotsi,[4] and Konstantin G. Kornev[1,a)]

[1]*School of Materials Science & Engineering, Clemson University, Clemson, South Carolina 29634, USA*
[2]*Department of Physics, Drexel University, Philadelphia, Pennsylvania 19104, USA*
[3]*Section of Endocrinology, Boston University School of Medicine, Boston, Massachusetts 02118, USA*
[4]*Department of Chemistry & Department of Materials Science & Engineering, Drexel University, Philadelphia, Pennsylvania 19104, USA*
[5]*Department of Bioengineering, Clemson University, Clemson, South Carolina 29634, USA*

(Received 9 April 2012; accepted 3 June 2012; published online 21 June 2012)

We report on the development of a multifunctional magnetic rotator that has been built and used during the last five years by two groups from Clemson and Drexel Universities studying the rheological properties of microdroplets. This magnetic rotator allows one to generate rotating magnetic fields in a broad frequency band, from hertz to tens kilohertz. We illustrate its flexibility and robustness by conducting the rheological studies of simple and polymeric fluids at the nano and microscale. First we reproduce a temperature-dependent viscosity of a synthetic oil used as a viscosity standard. Magnetic rotational spectroscopy with suspended nickel nanorods was used in these studies. As a second example, we converted the magnetic rotator into a pump with precise controlled flow modulation. Using multiwalled carbon nanotubes, we were able to estimate the shear modulus of sickle hemoglobin polymer. We believe that this multifunctional magnetic system will be useful not only for micro and nanorheological studies, but it will find much broader applications requiring remote controlled manipulation of micro and nanoobjects. © *2012 American Institute of Physics*. [http://dx.doi.org/10.1063/1.4729795]

I. INTRODUCTION

Actuation and rotation of magnetic materials by applying alternating current (ac) magnetic field is an attractive method to probe the materials mechanical properties. Many materials can be made magnetic by embedding magnetic micro and nanoparicles which are available on the market or can be produced in the laboratory (see, for review, Refs. 1–3). Magnetic nanoparticles with different shapes and surface functionalization are attractive candidates for the sensoric and diagnostic applications. Such applications call for the development of new devices providing controlled manipulation of the objects in question.[4–8] Depending on the method of field generation, these devices can be split into two groups.[9–11] One group employs permanent magnets fixed on a movable stage/holder which can be shaken or spun to produce an ac field.[10,11] Another group utilizes coils generating magnetic fields with a broad frequency band.[12–15]

The permanent magnets are attractive candidates because they provide high gradients of the magnetic field. When the stage with a magnet rotates or moves back and forth, the nanoparticles readily follow the generated field.[10,11,16–20] On the other hand, the frequency band generated by the moving stage is very narrow. This limits the application of permanent magnets.

Many practical applications require an ac field covering a broad frequency band. In this respect, electromagnets offer significant flexibility: the magnitude, direction, and frequency of the magnetic field can be remote controlled by simply changing the current on the magnetic coils.[13,21]

In optofluidic applications, when one needs to precisely control the rotation and simultaneous observation of the magnetic particles, the system has to meet the following criteria: (1) the size of the micro-rotator has to be small enough to place it under the microscope objectives; (2) the setup must be flexible to ensure an easy change of the setup configuration by rearranging the coils or changing the distance between them; (3) the magnitude and frequency of the magnetic field have to be remote controlled. Several groups have been working in the past years to apply electro-magnetic control in optofluidic devices.[13,15,21–29]

In this respect, rotating magnetic field deserves special attention.

Generation of the rotating magnetic field can be done with small Helmholtz coils having the cores measured in millimetres and even hundreds of micrometers.[24,30–32]

Magnetic rotators with small Helmholtz coils can provide the rotation frequency in the range between 1 Hz to 1 kHz and the ten millitesla field strength.[8,15,21,25,26,28,29,33] The strength and frequency of magnetic field are limited by the coil ability to support high currents. It was shown that small water-cooled magnetic coils can maintain sufficiently high rotating magnetic fields.[13]

In this paper, we report on the development of a multifunctional magnetic rotator that has been designed and implemented by two groups to study different biophysical and materials science phenomena. We show that using a rotating field, one can probe mechanical properties of materials that are difficult to analyze by any other available techniques.

a)Author to whom correspondence should be addressed. Electronic mail: kkornev@clemson.edu.

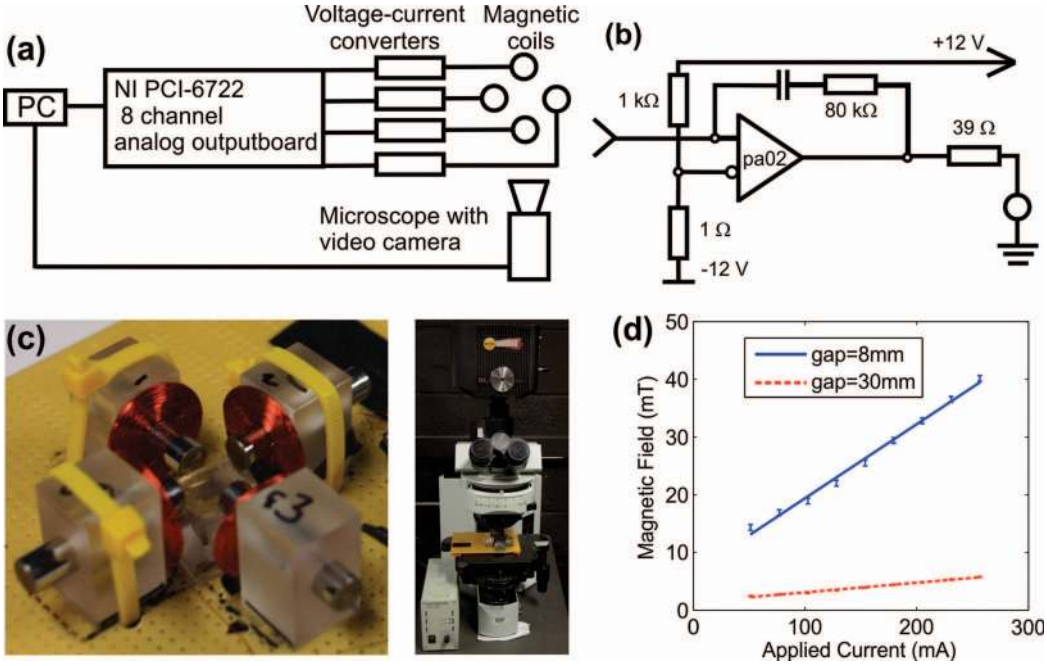

FIG. 1. (a) Circuit of magnetic rotator. (b) Circuit of the voltage-current converter. (c) An example of magnetic rotator. (d) Experimental measurements of the magnetic field in the middle of the two face-to-face placed coils as a function of applied current.

Below, we explain the features of the proposed magnetic rotator. This rotator satisfies all optofluidic requirements. Some examples illustrating the micro-rotator advantages are demonstrated.

II. DESIGN OF THE MAGNETIC ROTATOR

Compact and versatile magnetic rotator was designed and used with upright microscopes: Olympus BX51/MVX10/ inverted home-built microscope with Leica optics. The device circuit is shown in Fig. 1(a). In the schematic, we show the working head of the rotator that includes four solenoids with soft iron cores (Fig. 1(c)). In order to work with small optical cells that can be placed under a microscope, one needs sufficiently small solenoid coils with high inductance. We used 20.7 mm diameter and 1.5 mm thick coils (Solarbotics). The 6 mm diameter cylindrical cores made of soft iron were chosen long enough to deliver millitesla range fields, the length depends on the application. The solenoids were assembled on a stage under the microscope objective; see an example in Fig. 1(c).

The rotating magnetic field was generated using a waveform analog output PCI board (NI-PCI 6722) and custom 4-channel voltage-to-current converter. This NI-PCI 6722 board has 8 independent analog outputs and can produce signals with the frequencies up to 10 kHz. A LABVIEW 7 (NI) code allows one to generate four sinusoidal signals shifted by 90 degrees and smoothly converted to the voltage signal by an analog output board with a digitization frequency of about 200 kS/s per channel.

A circuit of the voltage-to-current converter is shown in Fig. 1(b). It is based on a 350 kHz, 5A power amplifier, PA02 Cirrus Logic, Inc. It is designed to drive the inductive loads and has a low crossover distortion. Using this highly integrated and relatively costly amplifier, one allows to keep the circuitry simple and any repair inexpensive. The generated current controls the strength and direction of the magnetic field in the field of view of the microscope.

NI LABVIEW Signal Express (http://www.ni.com/labview/signalexpress/) was chosen to design a software to control the operation of magnetic micro-rotator. This software allows one to precisely control the magnetic field and to simultaneously acquire images of the rotating objects during the experiments.

For the applications requiring stronger magnetic fields, we used E-66-100 coils (15 mm diameter and 8.5 mm thick, Magnetic Sensor Systems). In order to analyze the strength of magnetic field produced by these coils, two coils were placed face to face and the magnetic field was measured using the digital teslameter (133-DG GMW Inc.). The current-magnetic field curves are shown in Fig. 1(d) (the error bar represents a standard deviation from 3 measurements at each current). One confirms that placing the coils 8 mm apart, one can reach the 40 mT magnetic field. When the coil-to-coil distance was increased to 30 mm, the filed strength dropped down to 5 mT. A few millitesla fields are sufficient enough to rotate magnetic nanoparticles.[8,21]

In our experiments, we examined the performance of four, three, and two magnetic coils. The software developed in LABVIEW is able to produce three types of magnetic fields: rotating, pulsating, and dc fields. A microscope equipped with a camera is used to record the images and videos of the moving objects. Different signal shapes such as the dc, square, sinusoidal, or triangle signals can be generated with the developed device. The shape of the signal can be changed by setting up a formula for the signal shape or by uploading a

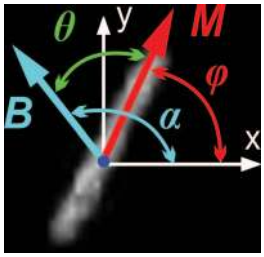

FIG. 2. A uniform magnetic field **B** rotates in a plane of this figure making angle α(t) with the reference X-axis. Magnetic moment of the nanorod, **M**, makes angle θ (t) with the field direction. Magnetic moment forms angle φ(t) with the reference X-axis.

data file with a defined signal into the LABVIEW program. The system was calibrated by sending the output signal from the LABVIEW program and measuring magnetic field at the center of the magnetic cell.

The designed system has a sufficient flexibility and can be used for different applications. Some examples are given below.

III. MEASURING A TEMPERATURE-DEPENDENT VISCOSITY OF A MICRODROPLET

A. Theory of nanorod rotation in liquids with constant viscosity

Consider a magnetic nanorod suspended in a liquid and subject to a rotating magnetic field, Fig. 2.

In order to derive an equation governing the nanorod rotation, it is convenient to count the nanorod revolutions with respect to the fixed system of coordinates, say, X-axis. The angle α specifies the direction of applied magnetic field **B** with respect to the reference X-axis. The drag force resists the nanorod rotation causing the nanorod to lag behind the field, making angle θ with vector **B** (Fig. 2). Since the applied field rotates at the constant rate, this angle depends linearly on time, $\alpha = 2\pi ft$, where f is the frequency of the rotating magnetic field. Therefore, if the magnetization vector **M** makes angle $\varphi(t)$ with the X-axis, this angle can be connected to $\alpha(t)$ and $\theta(t)$ as $\varphi(t) = 2\pi ft - \theta(t)$.

The torque balance equation reads $(\gamma d\varphi/dt)\mathbf{e} = \mathbf{M} \times \mathbf{B}$, where γ is the drag coefficient, and **e** is the unit vector directed perpendicularly to the plane of the nanorod rotation.[34,35] Substituting the definition of angle $\varphi(t)$ through angles $\alpha(t)$, and $\theta(t)$, the governing equation takes on the following form:[15]

$$\gamma\left(2\pi f - \frac{d\theta}{dt}\right) = MB\sin\theta. \tag{1}$$

The drag coefficient γ depends on the nanorod length l, its diameter d, and liquid viscosity η as[36]

$$\gamma = \frac{\eta l^3 \pi}{3\ln(l/d) - A}, \tag{2}$$

where $A \approx 2.4$ is a constant calculated in Ref. 36.

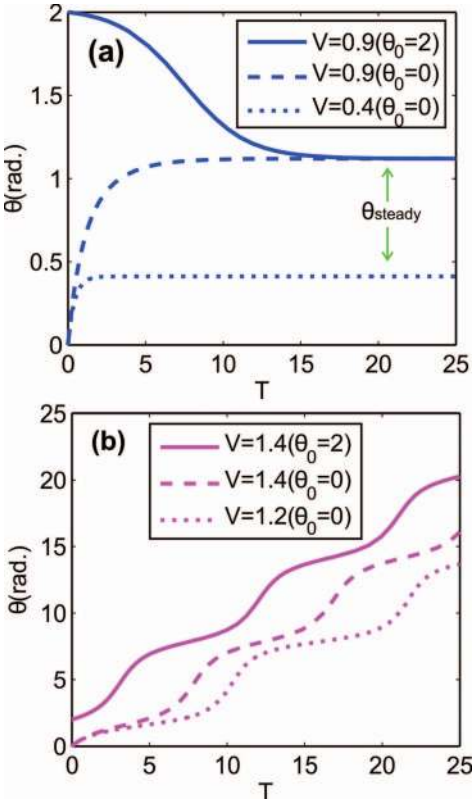

FIG. 3. Integral curves of Eq. (4) showing the solution behavior for different parameters $V(l, d, \eta, B, m, f)$ at different initial conditions θ_0. (a) V<1. (b) V>1.

It is convenient to introduce the dimensionless parameter V

$$V = \frac{2\pi\gamma f}{MB}, \tag{3}$$

and time $T = 2\pi ft$. The V-parameter characterizes the strength of the drag torque with respect to the magnetic torque. The denominator of Eq. (3) provides an upper estimate of the magnetic torque. The numerator provides an upper estimate of the drag torque assuming that the nanorod revolves with the frequency of applied field. With these parameters, the basic equation is rewritten as

$$\frac{d\theta}{dT} = \frac{1}{V}(V - \sin\theta). \tag{4}$$

Thus, only a single V-parameter carries all information about the materials properties of the nanorod and fluid. Changing the V-parameter, we can plot a set of trajectories of Eq. (4).

Effect of V – parameter. **V<1**. The dashed and dotted lines in Fig. 3(a) show the behavior of angle θ with time when the V-parameter is less than one, V = 0.9, V = 0.4 < 1, and the magnetic torque is stronger than the viscous drag. Initially, the nanorod and magnetic field are co-aligned, $\theta_0 = 0$. It can be seen that the angle θ increases and then stops changing. From this moment on, the nanorod starts rotating synchronously with the field making constant angle θ_{steady} with it. The greater the parameter V, the greater the constant θ_{steady}. According to Eq. (3), the V – parameter can be increased by

increasing the fluid viscosity or decreasing the field strength. Therefore, the changes of viscosity or magnetic field can be traced through the change of θ_{steady}.

Effect of initial nanorod orientation. **V<1**. The solid line in Fig. 3(a) corresponds to initial condition $\theta_0 = 2$. In this case, the magnetic force is stronger than the viscous drag, but the initial angle between the nanorod and the field is greater than $\pi/2$. According to Eq. (4), this initial condition makes the right hand side negative, i.e., the angle θ decreases in first moments of time. Magnetic field moves in positive direction, i.e., in the counterclockwise direction toward the direction where the initial magnetic moment is pointing to. On the other hand, the magnetic torque always turns the nanorod toward the field direction. These two simultaneous movements result in a decrease of angle θ. When the angle θ reaches the value V = sin θ, the derivative in Eq. (4) goes to zero and the angle reaches its steady state value θ_{steady}. Thus, for V<1, the initial orientation of the nanorods has no influence on the steady state angle θ_{steady}.

An interpretation of the theta-solutions becomes easier when we look at angle φ that the nanorod makes with the X-axis, $\varphi(t) = 2\pi ft - \theta(t)$ (Fig. 2). This angle can be measured experimentally by directly following the nanorod rotation with a camera and a microscope.

Fig. 4 shows the behavior of φ-solutions corresponding to the nanorod trajectory. Ethylene glycol is used as a carrying fluid. The angle φ was calculated as $\varphi(t) = \alpha(t) - \theta(t)$.

Fig. 4(a) shows a series of numerical solutions of Eq. (4). These φ-solutions are asymptotically linear functions of time: the slopes of solid lines and the corresponding lines with markers are the same and are equal to the frequency of the driving field and the frequency of rotating nanorod, respectively. These solutions describe a synchronous rotation of the nanorod with magnetic field when the nanorod makes a constant angle with the field direction during this rotation.

This numeric analysis suggests that when parameter V is smaller than one and magnetic torque dominates the drag torque, one can have a time independent solution of Eq. (4). The trajectories in Fig. 3(a) have constant asymptotes describing this type of solutions when the nanorod is picked up by magnetic field and rotates synchronously with the field. The phase lag between the field and nanorod becomes constant when derivative $d\theta/dT$ becomes zero. In this case, Eq. (4) is simplified to

$$\gamma 2\pi f = MB \sin\theta_{steady}. \tag{5}$$

Solving this equation for θ_{steady}, we notice that the solution exists if and only if the rotation frequency f is below the critical frequency:[15,35]

$$f_c = \frac{1}{2\pi}\frac{MB}{\gamma}. \tag{6}$$

Expressing the magnetic moment through the material magnetization m, $M = mv$, where $v = \frac{\pi d^2 l}{4}$ is the nanorod volume, and combining Equations (2) and (6), we notice that the dimensionless critical frequency f_d does not depend on the particular size of the nanorod, but only on the nanorod aspect ratio:

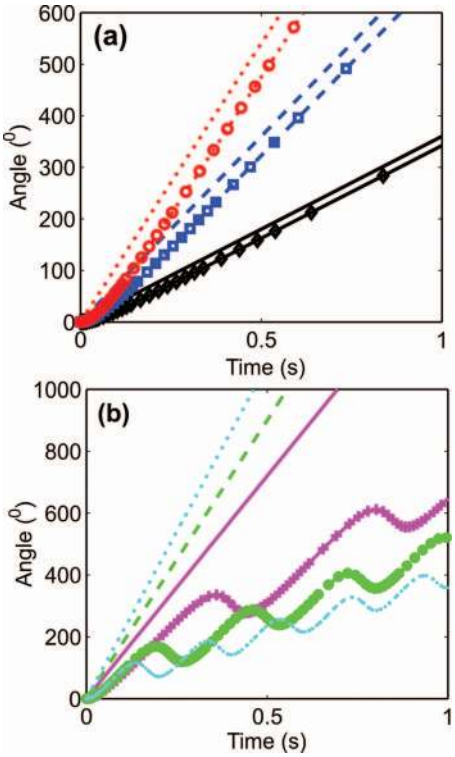

FIG. 4. (a) The φ-solutions of Eq. (4) for different driving frequencies of magnetic field. The upper straight lines correspond to the change of alpha-angles with frequencies f = 1 Hz (straight solid line), f = 2 Hz (straight dashed line), and f = 3 Hz (straight dotted line). The corresponding φ-solutions are marked with different symbols. The nanorod rotates synchronously with magnetic field at these frequencies. (b) The φ-solution of Eq. (4) for different driving frequencies of magnetic field. The upper straight lines correspond to the change of alpha-angles with frequencies f = 4 Hz (straight solid line), f = 5 Hz (straight dashed line), and f = 6 Hz (straight dotted line). The corresponding φ-solutions are marked with different symbols.

$$f_d = \frac{8\pi\eta f_c}{mB} = \frac{3\ln\left(\frac{l}{d}\right) - 2.4}{\left(\frac{l}{d}\right)^2}. \tag{7}$$

Indeed, the viscous torque in Eq. (1) is proportional to l^3, while the magnetic torque is proportional to $d^2 l$. Thus, these two torques compensate each other and the length scale is cancelled leading to a universal dependence (7). Fig. 5 illustrates the dependence of dimensionless critical frequency f_d on the nanorod aspect ratio. Understanding this universal behavior of nanorods is important for practical applications: the rheological properties of very small droplets can be studied at a fixed frequency by adjusting the aspect ratio of the nanorods.

V > 1. Three lines in Fig. 3(b) show the behavior of angle θ with time when the viscous drag is greater than the magnetic force and the nanorod cannot follow the applied magnetic field. When the V-parameter is greater than one, the solutions do not have any linear asymptote as time goes to infinity. All solutions change periodically: the right hand side of Eq. (4) is a periodic function of θ, hence the time derivative on the left hand side is also a periodic function. This behavior is illustrated by our numeric example when we increase the frequency up to f = 4 Hz. The linear solutions are turned into the oscillating solutions in Fig. 4(b).

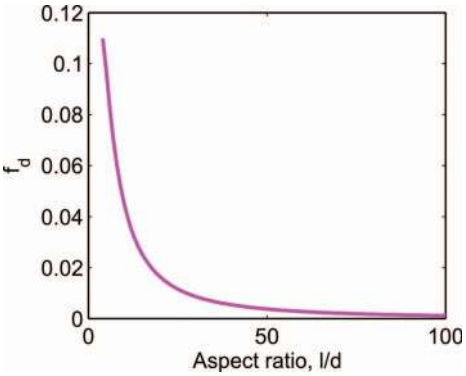

FIG. 5. Dependence of dimensionless critical frequency f_d on nanorod aspect ratio.

This theoretical analysis suggests that the nanorod behavior in a rotating magnetic field significantly depends on the revolution rate of magnetic field. One can distinguish synchronous rotation from asynchronous one by changing the rotation rate of the magnetic field. The critical frequency is an important parameter which is easy to measure experimentally by detecting a moment when the nanorod starts oscillating and slows down its rotation while the operator increases the frequency of the driving field. Obtaining this parameter from experiments, one can infer the materials parameters from Eq. (7). Therefore, knowing the critical frequency and geometrical parameters of the nanorod, one can measure either fluid viscosity (provided that the magnetic moment M is known) or the nanorod magnetic moment (provided that the fluid viscosity is known).[8,15] Equation (7) is the fundamental equation of magnetic rotational spectroscopy (MRS) for the analysis of viscous fluids with nanorods.[15,37]

B. Experiments and discussion

In the materials science applications, when a synthesized polymer is produced in a miniscule amount and the droplet size is measured in micrometers, the standard rheological instruments fall short to characterize the material. The MRS appears attractive because it provides a way to extract the rheological parameters of microdroplets by studying the rotational features of magnetic nanorods.[38]

In order to illustrate the robustness of the designed microrotator, we studied a temperature-dependent viscosity of microdroplets. Nickel nanorods were synthesized by using electrochemical template synthesis as described in Refs. 8 and 39. A viscosity standard liquid S600 (Cannon Instrument Company) was used in these experiments. Viscosity of this liquid depends on the temperature. The temperature-viscosity curve is shown in Fig. 6(a). This curve was generated using the table provided by the vendor with the data points marked by squares.

Experimentally, the critical frequency was determined by increasing the frequency of the driving magnetic field and measuring the frequency of the nanorod rotation. Image tracking procedures were used to obtain the rate of rotation of magnetic nanorods (Video Spot Tracker; http://cismm.cs.unc.edu/downloads/). Two coils of the magnetic rotator were fixed under the objective of BX-51 Olympus microscope (Fig. 1(c)). In order to produce a rotating magnetic field, two sinusoidal signals were sent to the coils with 90 degrees phase difference between them (Fig. 6(b)). This phase shift allows one to generate a rotating magnetic field. The strength of the magnetic field was determined by the amplitude of the sinusoidal signal which was set in the LABVIEW program. The system allows one to change the strength of magnetic field during the experiment.

A 10 μl droplet with the suspended Ni nanorods was placed on the insulated flexible heater made of a polymide film (KA-808, Omegalux). A DC Regulated Power Supply (CSI12001X, Circuit Specialists) was connected to the film and was used to control the temperature of the film. The surface temperature was measured with a thermocouple connected to the temperature controller (TC-3300, CAL Controls LTD). The drop was placed on the film and investigated under the 50× objective of the BX-51 Olympus microscope. We applied the dark field microscopy technique to detect the 200 nm nanorods which were not visible in the bright field.[40] A SPOT videocamera (SPOT Imaging Solutions, Inc.) was used for filming the rotating nanorods. A high speed digital camera (Motion Pro X3, Red Lake, FL) was used to capture the

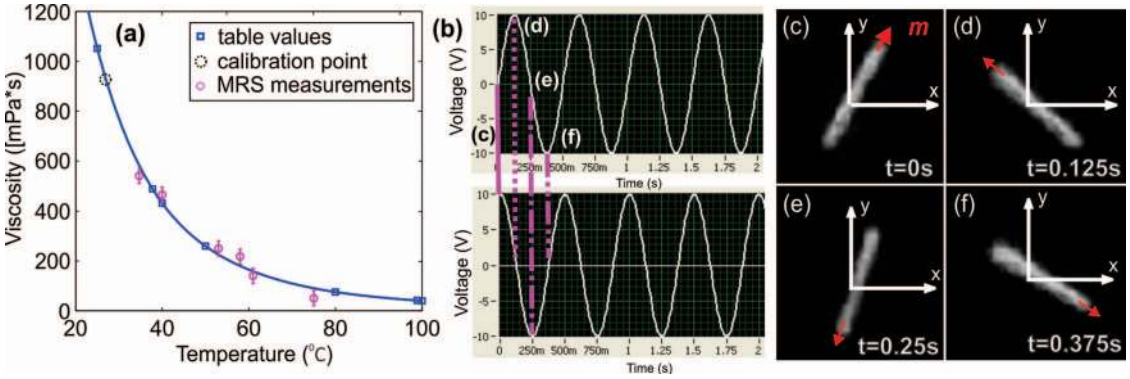

FIG. 6. (a) Viscosity of the viscosity standard liquid S600 measured by rotation of the nanorods with different aspect ratios; squares and blue line show the table values of the viscosity; open circles show measured viscosity from 5 independent experiments with nanorods of different aspect ratios. A data point corresponding to the 927.5 mPa · s viscosity was used to obtain constant $\chi = 290$. (b) Two sinusoidal signals sent to two coils at the time moments (c)–(f). Following the generated rotating field, the Ni nanorod rotates counterclockwise at 2 Hz frequency.

images of the rotating magnetic nanorods at frequencies higher than 25 Hz. The captured videos were analyzed manually using VIRTUALDUB software (http://www.virtualdub.org). Snapshots of a single rotating nanorod are shown in Figs. 2(c)–2(f). The recorded videos were used for the determination of a critical frequency of a particular nanorod. Knowing the critical frequencies, we obtained the magnetic moments of the nanorods and calculated the viscosity using Eq. (7).

To obtain magnetic moments of nanorods with different aspect ratios, we used the scaling arguments and represented magnetic moment in the form $M = VB\chi/\mu_0$, where V is the nanorod volume, μ_0 is the magnetic permeability of vacuum, and χ is a constant to be determined. Plugging this formula into Eq. (7) and solving for χ, one obtains χ - constant as a function of the critical frequency f_c, the fluid viscosity, and geometrical parameters of the nanorod.

We heated the drop up to 26.9 °C and used the calibrated viscosity $\eta = 927.5$ mPa · s (a dotted circle in Fig. 6(a)) given by the vendor. First, we experimentally determined f_c, the frequency at which the nanorod stopped rotating synchronously with the magnetic field. This viscosity value was used to obtain constant $\chi = 290$. Then the temperature of the substrate was raised up and a critical frequency was measured at six different temperatures for different nanorods. When the critical frequencies were determined, the viscosity was calculated using Eq. (7). The results of the viscosity measurements during the temperature rise (circles in Fig. 6(a)) are in a very good agreement with the values provided by the vendor. Therefore, this analysis confirms that the MRS with the designed magnetic rotator provides correct viscosity data, hence the instrument can work as a nanorheological viscometer.

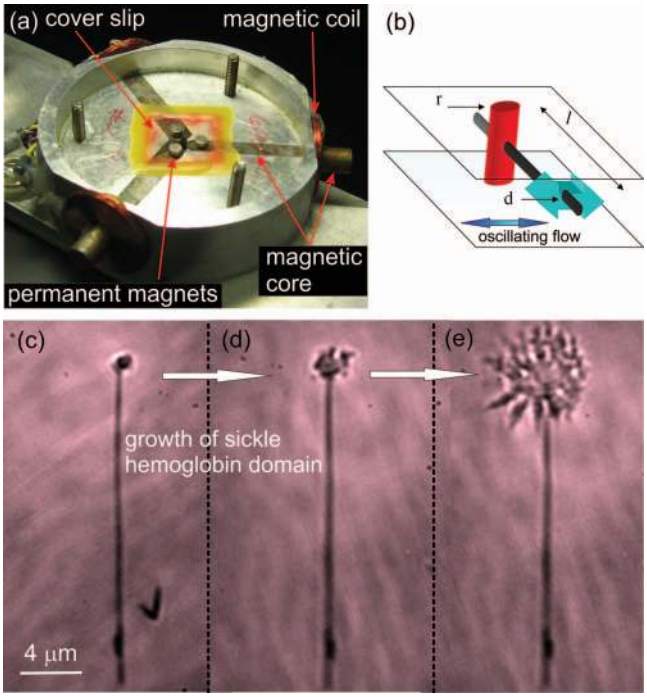

FIG. 7. (a) Schematic of the setup for measurements of shear modulus of polymeric filaments. (b) Schematic of a carbon nanotube embedded into the column of sickle cell hemoglobin. (c)–(e) Three images showing the growth of sickle hemoglobin domain initiated by the laser pulse. The black spot corresponds to the cross-section of a nucleating polymerized domain which is almost circular in the cross-section. The nanotube is directed parallel to the coverslips. One end of the nanotube is fixed by the polymerized domain and the rest of the nanotube is exposed to non-polymerized fluid. As the polymerized domain expands, it creates the side dendrites and the column is no longer circular in cross section.

IV. MEASURING THE MICRO RIGIDITY OF SICKLE HEMOGLOBIN POLYMER

This microrotator found another application in biophysical research related to the analysis of the mechanisms of micro-rigidity of sickle cell hemoglobin (HbS). This polymer is very rigid, its elastic modulus is measured in megapascals.[41] Therefore, the widely used biophysical techniques based on laser tweezers are not applicable here. The AFM based approaches are also questionable because the polymers are metastable: HbS is prone to a spontaneous polymerization when the concentration of deoxyHbS exceeds a well-defined level.[42] In biophysical experiments, a laser photolysis[43] was used to initiate nucleation of sickle hemoglobin polymer. Polymer nucleation and subsequent hardening occurs through the domain formation. The domain size can be controlled by the diameter of the laser beam but typically, the domains of interest are less than 7 μm in diameter, which is approximately equal to the size of the red blood cell. To study these small domains, we employed magnetic carbon nanotubes.[15,44] Aquesous suspensions of carbon nanotubes loaded with magnetic particles were produced as described in Ref. 15. The 200 nm diameter nanotubes were produced at Drexel University by non-catalytic chemical vapour deposition (CVD) using commercial alumina membranes (Whatman Anodisc, 13 mm in diameter, nominal pore diameter 200 ± 20 nm; 60 μm thickness) as templates.[15,45–48] To fill nanotubes with magnetic particles, we used a commercially available organic-based (EMG 911) ferrofluid (Ferrotec Corporation), which carries magnetite (Fe_3O_4) particles with a characteristic diameter of 10-15 nm. Transmission electron microscopy analysis has demonstrated a uniform loading of nanotubes with nanoparticles.[15,44]

Two coverslips (number 1, Fisher Scientific) were used to create a 15 μm thick microchannel (Figs. 7(a) and 7(b)). The microchannel was filled with the hemoglobin solution with suspended nanotubes. Hemoglobin was purified by column chromatography as previously described[49] and prepared in 0.15 M phosphate buffer, pH = 7.35. Samples also contained 0.50 M sodium dithionite that acted as an oxygen scavenger.[50] Concentrations were determined by diluting 2 μl hemoglobin solution into 6 ml phosphate buffer and measuring spectra on an HP8452 diode array spectrophotometer. Samples were prepared in a glove box filled with humidified CO. The measurements were performed on a custom made microscope with a horizontal stage. The beam of the 150 W xenon arc lamp passed through an Acton monochromator. Condenser and objective were both Leitz 32× long distance objectives.

In order to estimate the elastic properties of the polymerized sickle hemoglobin, the 20 μm long nanotubes were fixed by the polymer domain from one end (Figs. 7(b) and 7(c)). This nanotube fixation was achieved by illuminating the HbS

solution with the laser beam (5 W 488-nm Spectra Physics 164 argon ion laser) to ensure that the polymer domain has nucleated at the end of the nanotube. The growth of sickle hemoglobin polymers by illuminating carboxyhemoglobin with a 488 nm laser is described elsewhere.[49] The polymer domain formed a cylindrical column bridging both coverslips through the whole gap between them. Therefore, the column has 15 μm length and its radius (r, Fig. 7(b)) was controlled by the diameter of the laser beam.

Applying rotating magnetic field as explained in Sec. III, we attempted to rotate the nanotube to create a torque on the polymerized cylinder. However, the polymerized cylinder appeared strong and did not let the nanotube rotate. We therefore changed the strategy but used the same magnetic rotator.

We made three trenches converging to the center of the stage. Magnetic cores were buried into trenches and three coils were placed to the core open ends, Fig. 7(a). The microchannel with a polymer solution and suspended nanotubes was placed at the center of the stage so that the ends of magnetic cores formed an external ring. The 2 mm diameter rare-earth magnets (Armstrong Magnetics, Inc) were placed on top of the coverslip and accurately glued to it as shown in Fig. 7(a).

Applying either an inward or an outward bias on each permanent magnet, we were able to deform the top coverslip. This bias pushed the magnet either toward or outward the coil. Therefore, a periodic modulation of the gap thickness allowed one to suck/squeeze the fluid in/out creating a unidirectional in-plane flow parallel to the cover slips. One cannot predict where the nanotube will be caught and fixed by the laser, therefore, having a three-coiled rotator configuration, one can control the flow direction by applying different phase-shifted signals as explained above.

The flow was characterized by the particle imaging velocimetry (PIV) using the 200 nm polystyrene beads (FluoroSpheres, Molecular Probes) added to the solution, so that the flow velocity was measured at each point along the nanotube. Photron PCI-512 camera was used for recording the video. Data collection and signal timing were integrated through a PC running LABVIEW program. Typically, we applied the 0.5 Hz frequency ac field to deform the coverslip. This modulation provided the flow with an average velocity $\upsilon \cong 30$ μm/s.

When a flow was created, we observed a displacement of the free end of the nanotube, i.e., the nanotube rotated by a small angle about the axis of polymerized column where the fixed end was buried. This rotation was caused by the drag force acting on the cantilevered nanotube. As known from fluid mechanics,[36] the drag force F acting on the rigid rod placed in a uniform stream moving with velocity υ is written as

$$F = \frac{4\pi\eta l}{\ln(l/d)}\upsilon. \tag{8}$$

Since the stream velocity was measured by PIV, and other parameters were measured independently, the force was completely specified. Once the force is known, the torque on the polymerized column is defined as $\mathbf{M = \mathit{Fl/2}}$. This torque is counterbalanced by the elastic traction of the polymerized column. Modelling the column as a circular cylinder of radius r, and length L, the elastic torque is expressed as $\mathbf{M = \pi r^4 G\alpha/(2L)}$, where G is the shear modulus of the polymerized domain and α is the twisting angle. Balancing the drag torque and elastic torque and solving for shear modulus G, we obtain

$$G = \frac{FLl}{\pi r^4 \alpha}. \tag{9}$$

Plugging the geometrical parameters of the nanotube, $d = 200$ nm, $l = 20$ μm, the stream velocity $\upsilon = 30$ μm/s, and the viscosity of aqueous solution of hemoglobin with c = 27 g/dl (decilitre) concentration $\eta = 7$ mPa $\cdot$ s,[51] we estimated the drag force from Eq. (8). The maximum achievable force in our experiments was $F = 0.01$ nN. The twisting angle α, corresponding to the angle by which the nanotube was displaced, was measured independently from the images. We obtained $\alpha \cong 0.1^\circ$. The distance between the coverslips was $L \cong 15$ μm and the radius of polymerized domain was $r \cong 1.4$-1.5 μm. Substituting these parameters in Eq. (9), we estimated the shear modulus of the polymerized hemoglobin domain as $G \cong 110$-150 KPa. Assuming that the Poisson ratio of the polymer is about $\frac{1}{2}$, the shear modulus should be about three times smaller than the Young modulus E. This estimate is in excellent agreement with our previous data obtained by the different method, where we estimated the Young modulus as E $\cong$ 300-500 KPa.[43]

This experiment illustrates the device flexibility: one can easily change the setup configuration keeping the same driving circuit. In our groups we use the same device to measure the bending and torsion modules of microfibers and nanofiber yarns, to study kinetics of photopolymerization by the MSR,[21] to study kinetics of nanoparticle chaining, and to pump fluids through microfluidic devices. Therefore, magnetic microrotator offers many new opportunities to study flow and rheological characteristics of microdroplets, nano and microfibers, ribbons and flakes in optofluidic devices.

V. CONCLUSIONS

We developed a multifunctional magnetic rotator that allows one to generate rotating magnetic fields in a broad frequency band, from hertz to tens kilohertz. During the last five years, two groups from Clemson and Drexel Universities used this device for different nano and microfluidic applications. In particular, this magnetic rotator was used for the rheological studies of simple and polymeric fluids at the nano and microscale. As an illustration of the system robustness and flexibility, we demonstrated two experiments. We employed this system to study a temperature-dependent viscosity of a synthetic oil used as a viscosity standard. Magnetic rotational spectroscopy with suspended nickel nanorods was used for these purposes. It was shown that the MRS-based results perfectly reproduced a temperature dependence of the oil viscosity during the heating process. The same magnetic system was used to pump hemoglobin solution through a microfluidic channel with precise controlled flow modulation. Using multiwalled carbon nanotubes, we were able to estimate the shear modulus of sickle hemoglobin polymer.

We believe that this multifunctional magnetic system will be useful not only for micro and nanorheological studies, but it will find much broader applications requiring remote controlled manipulation of micro and nanoobjects.

ACKNOWLEDGMENTS

We thank Gelester Baskett for the assistance with the synthesis of Ni nanorods, and David White for his help at different stages of this project. The authors thank Professor F. A. Ferrone for suggesting to study hemoglobin rheology and for general advice during the project. The authors are grateful for the financial support of National Science Foundation, Grant EFRI 0937985 and National Institutes of Health Grants R01HL057549 and P01HL058512.

[1] Int. J. Mol. Sci. (Special Issue - Magnetic Nanoparticles) **12**, (2011).
[2] D. L. Graham, H. A. Ferreira, and P. P. Freitas, Trends Biotechnol. **22**, 455–462 (2004).
[3] K. M. Krishnan, IEEE Trans. Magn. **46**, 2523–2558 (2010).
[4] C. Wilhelm, Phys. Rev. Lett. **101**, 028101 (2008).
[5] X. Q. Chi, D. T. Huang, Z. H. Zhao, Z. J. Zhou, Z. Y. Yin, and J. H. Gao, Biomaterials **33**, 189–206 (2012).
[6] J. Gao and B. Xu, Nano Today **4**, 37–51 (2009).
[7] S. Z. Malynych, A. Tokarev, S. Hudson, G. Chumanov, J. Ballato, and K. G. Kornev, J. Magn. Magn. Mater. **322**, 1894–1897 (2010).
[8] A. Tokarev, B. Rubin, M. Bedford, and K. G. Kornev, AIP Conf. Proc. **1311**, 204–209 (2010).
[9] D. Choi, A. Fung, H. Moon, D. Ho, Y. Chen, E. Kan, Y. Rheem, B. Yoo, and N. Myung, Biomed. Microdevices **9**, 143–148 (2007).
[10] A. Celedon, C. M. Hale, and D. Wirtz, Biophys. J. **101**, 1880–1886 (2011).
[11] B. A. Evans, A. R. Shields, R. L. Carroll, S. Washburn, M. R. Falvo, and R. Superfine, Nano Lett. **7**, 1428–1434 (2007).
[12] B. G. Hosu, K. Jakab, P. Banki, F. I. Toth, and G. Forgacs, Rev. Sci. Instrum. **74**, 4158–4163 (2003).
[13] B. Frka-Petesic, K. Erglis, J. F. Berret, A. Cebers, V. Dupuis, J. Fresnais, O. Sandre, and R. Perzynski, J. Magn. Magn. Mater. **323**, 1309–1313 (2011).
[14] K. Paivo, S. Irene, H. M. Brandon, and K. Raoul, Appl. Phys. Lett. **97**, 223701 (2010).
[15] G. Korneva, H. Ye, Y. Gogotsi, D. Halverson, G. Friedman, J.-C. Bradley, and K. G. Kornev, Nano Lett. **5**, 879–884 (2005).
[16] A. K. Vuppu, A. A. Garcia, and M. A. Hayes, Langmuir **19**, 8646–8653 (2003).
[17] A. R. Bausch, W. Möller, and E. Sackmann, Biophys. J. **76**, 573–579 (1999).
[18] F. Mosconi, J. F. Allemand, and V. Croquette, Rev. Sci. Instrum. **82**, 034302 (2011).
[19] A. Celedon, I. M. Nodelman, B. Wildt, R. Dewan, P. Searson, D. Wirtz, G. D. Bowman, and S. X. Sun, Nano Lett. **9**, 1720–1725 (2009).
[20] A. Hultgren, M. Tanase, C. S. Chen, G. J. Meyer, and D. H. Reich, J. Appl. Phys. **93**, 7554–7556 (2003).
[21] A. Tokarev, I. Luzinov, J. R. Owens, and K. G. Kornev, Langmuir, DOI: 10.1021/la3019474 (2012).
[22] B. B. Yellen, O. Hovorka, and G. Friedman, Proc. Natl. Acad. Sci. U.S.A. **102**, 8860–8864 (2005).
[23] C. Gosse and V. Croquette, Biophys. J. **82**, 3314–3329 (2002).
[24] M. Barbic, J. Magn. Magn. Mater. **249**, 357–367 (2002).
[25] L. G. Wilson and W. C. K. Poon, Phys. Chem. Chem. Phys. **13**, 10617–10630 (2011).
[26] J. Llandro, J. J. Palfreyman, A. Ionescu, and C. H. W. Barnes, Med. Biol. Eng. Comput. **48**, 977–998 (2010).
[27] P. Tierno, J. Claret, F. Sagues, and A. Cemacrbers, Phys. Rev. E **79**, 021501 (2009).
[28] K. Keshoju, H. Xing, and L. Sun, Appl. Phys. Lett. **91**, 123114 (2007).
[29] C. Wilhelm, F. Gazeau, and J. C. Bacri, Phys. Rev. E **67**, 061908 (2003).
[30] M. Barbic, J. J. Mock, A. P. Gray, and S. Schultz, Appl. Phys. Lett. **79**, 1897–1899 (2001).
[31] M. K. Yapici and J. Zou, Microsyst. Technol. **14**, 881–891 (2008).
[32] M. K. Yapici, A. E. Ozmetin, J. Zou, and D. G. Naugle, Sens. Actuators, A **144**, 213–221 (2008).
[33] B. H. McNaughton, K. A. Kehbein, J. N. Anker, and R. Kopelman, J. Phys. Chem. B **110**, 18958–18964 (2006).
[34] L. D. Landau and E. M. Lifshitz, *Electrodynamics of Continuous Media* (Pergamon, Oxford, 1960).
[35] E. Blums, A. Cebers, and M. M. Maiorov, *Magnetic Fluids* (Walter de Gruyter, New York, 1997).
[36] M. Doi and S. F. Edwards, *The Theory of Polymer Dynamics* (Clarendon Press, Oxford, 1988).
[37] J. Frenkel, *Kinetic Theory of Liquids* (Dover Publications, New York, 1955).
[38] T. A. Waigh, Rep. Progr. Phys. **68**, 685 (2005).
[39] A. K. Bentley, M. Farhoud, A. B. Ellis, G. C. Lisensky, A. M. L. Nickel, and W. C. Crone, J. Chem. Educ. **82**, 765–768 (2005).
[40] S. Innoue, *Video Microscopy: The Fundamentals (Language of Science)* (Springer, New York, 1997).
[41] A. Aprelev, Z. H. Liu, and F. A. Ferrone, Biophys. J. **101**, 885–891 (2011).
[42] A. Aprelev, W. J. Weng, M. Zakharov, M. Rotter, D. Yosmanovich, S. Kwong, R. W. Briehl, and F. A. Ferrone, J. Mol. Biol. **369**, 1170–1174 (2007).
[43] M. N. Zakharov, A. Aprelev, M. S. Turner, and F. A. Ferrone, Biophys. J. **99**, 1149–1156 (2010).
[44] K. G. Kornev, D. Halverson, G. Korneva, Y. Gogotsi, and G. Fridman, Appl. Phys. Lett. **92**, 233117 (2008).
[45] T. Kyotani, L. F. Tsai, and A. Tomita, Chem. Mater. **7**, 1427–1428 (1995).
[46] M. P. Rossi, H. Ye, Y. Gogotsi, S. Babu, P. Ndungu, and J.-C. Bradley, Nano Lett. **4**, 989–993 (2004).
[47] D. Mattia, H. H. Bau, and Y. Gogotsi, Langmuir **22**, 1789–1794 (2006).
[48] M. P. Rossi, Y. Gogotsi, and K. G. Kornev, Langmuir **25**, 2804–2810 (2009).
[49] F. A. Ferrone, J. Hofrichter, and W. A. Eaton, J. Mol. Biol. **183**, 591–610 (1985).
[50] O. Galkin, R. L. Nagel, and P. G. Vekilov, J. Mol. Biol. **365**, 425–439 (2007).
[51] P. D. Ross and A. P. Minton, Biochem. Biophys. Res. Commun. **76**, 971–976 (1977).